

# Internal Model-Based Feedback Control Design For Inversion-Free Feedforward Rate-Dependent Hysteresis Compensation of Piezoelectric Cantilever Actuator

Mohammad Al Janaideh<sup>1</sup> Micky Rakotondrabe<sup>2\*</sup>, Isam Al-Darabsah<sup>3</sup>, and Omar Aljanaideh<sup>2,4</sup>

<sup>1</sup>*Mechanical Engineering department, Memorial University of Newfoundland, St. John's, NL, A1B 3X5, Canada*

<sup>2</sup>*Automatic Control and Micro-Mecatronic Systems department, FEMTO-ST inst., University of Burgundy Franche-Comté, Besançon France.*

<sup>3</sup>*Mathematics and Statistics department, Memorial University of Newfoundland, St. John's, NL, A1C 5S7, Canada.*

<sup>4</sup>*Electrical Engineering department, University of Washington, Seattle, WA, USA.*

*\*corresponding author email mrakoton@femto-st.fr, fax +33 381 402 810*

---

## Abstract

This study proposes a new rate-dependent feedforward compensator for compensation of hysteresis nonlinearities in smart materials-based actuators without considering the analytical inverse model. The proposed rate-dependent compensator is constructed with the inverse multiplicative structure of the rate-dependent Prandtl-Ishlinskii (RDPI) model. The study also presents an investigation for the compensation error when the proposed compensator is applied in an open-loop feedforward manner. Then, an internal model-based feedback control design is applied with the proposed feedforward compensator to a piezoelectric cantilever actuator. The experimental results illustrate that the proposed feedforward-feedback control scheme can be used in micro-positioning motion control applications to enhance the tracking performance of the piezoelectric cantilever actuator under different operating conditions.

*Key words:* Piezoelectric actuators, rate-dependent hysteresis, Prandtl-Ishlinskii modeling, inversion-free compensation method, feedforward-feedback scheme, internal model control.

---

## 1 Introduction

Smart materials-based actuators such as Shape Memory Alloys (SMAs), piezoelectric and magnetostrictive actuators are attractive for applications that require positioning/manipulating objects at micro and nano-scale levels [1–3]. However, these actuators exhibit rate-dependent hysteresis nonlinearities that increase as the frequency of the applied input increases. Such nonlinearities are known to cause oscillations and instabilities in open and closed-loop systems [4, 5]. Different feedback control methods have been used to reduce the hysteresis nonlinearities of smart materials-based actuators. However, synthesizing feedback controllers at high excitations of input frequency is a challenging task due to the presence of rate-dependent hysteresis nonlinearities. Furthermore, applying high levels of input amplitude to these actuators contributes asymmetric hysteresis nonlinearities which necessitate adequate consideration for the effects of input amplitude [6, 7].

Implementing a rate-dependent compensator to reduce the effects of the rate-dependent hysteresis nonlinearities of a smart material-based actuator strongly facilitates the design of a linear or nonlinear feedback controllers. A few studies have suggested nonlinear control design such as adaptive control [8], energy-based control [9], hybrid control [10], optimal control [11], robust control [12, 13], and sliding-mode control [14] to cancel-out hysteresis nonlinearities of smart materials-based actuators. Compared to other methodologies, a cascade arrangement of a rate-dependent hysteresis model and its rate-dependent inverse is known as an effective methodology for compensation of hysteresis nonlinearities in real-time system [4, 15]. However, deriving an analytical inverse model that is adaptive with the frequency involves difficulties that are associated with mathematical properties of the hysteresis model itself.

The Preisach and Prandtl-Ishlinskii models are among the most popular hysteresis models that have been used with their inverse models for modeling and compensation of hysteresis nonlinearities of smart material-based actuators [3, 6, 15–21]. Because of the exact inversion of the model, the Prandtl-Ishlinskii model is considered attractive for compensation of hysteresis nonlinearities in real-time applications [20, 21]. However, the Prandtl-Ishlinskii model is rate-independent hysteresis model. This problem has been addressed in [22] where the model and its inverse were extended to new versions that account for the rate of the applied input. The RDPI model and its inverse were applied for characterization and compensation of rate-dependent hysteresis nonlinearities of magnetostrictive [23] and piezoelectric [22] actuators. However, the inverse RDPI model is available only when the rate-dependent threshold function satisfies the dilation condition [22].

The mathematical conditions that are necessary to formulate an invertible

RDPI model can be relaxed with the inverse multiplicative structure of the hysteresis model. Thus, the hysteresis compensator can be obtained by restructuring the hysteresis model that characterizes the hysteresis nonlinearities. This technique has been successfully applied to compensate for the hysteresis nonlinearities of the Bouc-Wen model [24], the generalized Bouc-Wen model [25], multivariable Bouc-Wen [26], the Preisach model [27, 28], the Prandtl-Ishlinskii model [20], the multivariable Prandtl-Ishlinskii model [21] and recently the RDPI model [29].

Although employing the inverse multiplicative structure is effective for compensation of hysteresis nonlinearities in open-loop feedforward manner, synthesizing feedback control techniques is essential to maintain or to improve the tracking performance in presence of internal and external disturbances such as: modeling uncertainties and environmental influence. However, feedback control designs necessitate adequate consideration for the compensation error of the feedforward compensator and the boundedness of compensation error. Thus, exploring the compensation error facilitates applying feedback control architectures such as proportional-integral-derivative controller, internal model-based feedback, hybrid control, or robust control, as examples, with the inverse multiplicative structure. This study presents a feedforward and feedback control scheme to improve the performances of smart materials based actuators over a wide range of input frequency. The feedforward controller (compensator) is based on the combination of the inverse multiplicative structure and the RDPI model and a thorough analysis of the tracking error is developed. The feedback controller is based on the internal model control scheme which permits to consider remaining compensation errors, model uncertainties and eventual external disturbance. Finally, the whole is applied to a piezoelectric cantilever actuator that is characterized by a rate-dependent hysteresis, a creep phenomenon and badly damped oscillations. The main contributions of the study can be summarized as follows:

- A rate-dependent feedforward hysteresis compensator for compensation of hysteresis nonlinearities of smart materials-based actuators without formulating inverse rate-dependent models is derived. The compensator is based on the rearrangement of a rate-dependent Prandtl-Ishlinskii (RDPI) model. Additionally to the Lipschitz continuity analysis of the model, we also investigate the bound of the tracking error from the compensation as well as the condition on the sampling period to make this bound valuable.
- From a linear model with error derived from the previous analysis, we augment the feedforward control system by a feedback controller. The aim of this feedback is to cancel the remaining error and to reject eventual disturbance that a feedforward would not allow. For that we suggest the internal model control (IMC) which permits to consider model uncertainties in the new linear model, additionally to the error and to the external disturbance.
- Finally, the proposed RDPI-feedforward and IMC-feedback control scheme

have been applied to a piezoelectric actuator classically used in micromanipulation applications. The efficiency of the feedforward-feedback scheme is particularly compared with the result from a feedback-only scheme, and is shown to demonstrate higher bandwidth.

The paper is organized as follows. Section II includes a description for the proposed compensation scheme and the formulation of RDPI model. In this section, the discrete RDPI model is also presented with the Lipschitz continuity property. Section III introduces the development of rate-dependent feedforward compensator on the basis of the inverse multiplicative scheme. This section also presents the boundedness of the error between the reference input and the output of the RDPI model when the proposed compensator is applied. Section VI is devoted to the application to a piezoelectric cantilever actuator. Its characterization, RDPI modeling and RDPI compensation are detailed in the same section. Section V presents synthesizing and applying of an internal model-based feedback control design to enhance the tracking performance of the compensated piezoelectric cantilever actuator. The conclusions of the paper are summarized in Section VI.

## 2 Background

Among the available smart material-based actuators, SMAs, magnetostrictive and piezoelectric types are considered the most popular for micro- and nano- positioning tasks. Due to their fine resolution and fast response, piezoelectric actuators for example, are employed in atomic force microscopy and also for manipulating small objects at micro- and nano- scale [3]. SMAs are another example of smart material-based actuators that are attractive for applications where flexibility and generation of large deformations are required. These actuators are integrated in the modern aircraft wings and the buildings structures to resist earthquakes vibrations [1, 30, 31]. These actuators show rate-dependent hysteresis nonlinearities between applied harmonic input and output displacement [32]. Such nonlinearities are considered relatively rate-independent at shallow levels of input frequency. However, applying harmonic input at high excitations of input frequency contributes a significant increase in the hysteresis nonlinearities. These nonlinearities cause high positioning errors and instabilities in the closed-loop control systems. Enhancing the tracking performance of smart material-based actuators necessitates selecting an appropriate model that can account for the hysteresis nonlinearities that these actuators exhibit. The Prandtl-Ishlinskii model is a flexible hysteresis model that can describe rate-independent as well as rate-dependent hysteresis properties of smart material-based actuators. The mathematical formulation of this model is presented in this section along with investigation for the Lipschitz continuity property of the model.

## 2.1 The RDPI model

A rate-dependent version of the Prandtl-Ishlinskii model has been proposed in [22, 23] for characterizing the rate-dependent hysteresis nonlinearities of magnetostrictive and piezoelectric actuators. The model is represented as a summation of weighted rate-dependent play operators. Each of these operators integrates a rate-dependent threshold that is formulated as a function of the input rate. We deal with real absolutely continuous functions that are defined on the interval  $(0, T)$ , such that the space of these functions can be denoted by  $AC(0, T)$ . Let us consider also the input  $z(t) \in AC(0, T)$ . For  $i = 0, 1, 2, \dots, n$ , where  $n \in \mathbb{N}$  is an integer, the  $r_i(\dot{z}(t)) \in AC(0, T)$  are considered as thresholds such that

$$0 = r_0(\dot{z}(t)) \leq r_1(\dot{z}(t)) \leq r_2(\dot{z}(t)) \leq \dots \leq r_n(\dot{z}(t)). \quad (1)$$

In addition,  $\Phi_{r_i(\dot{z}(t))}[z](t)$  is a rate-dependent play operator that has an output  $\xi_i(t)$  if

$$\xi_i(t) = \Phi_{r_i(\dot{z}(t))}[z](t). \quad (2)$$

Then, for an input  $z(t)$  and threshold functions  $r_i(\dot{z}(t))$  which are piecewise linear in each interval of a partition  $0 = t_0 < t_1 < \dots < t_l = T$  such that  $l \in \mathbb{N}$  is an integer, and given an initial condition  $\xi_i(0) = \max(z(0) - r_i(0), \min(z(0) + r_i(0), x_i))$ , the output of the rate-dependent play operator for  $t \in [t_{j-1}, t_j]$  is expressed as [22]

$$\xi_i(t) = \max\{z(t) - r_i(\dot{z}(t)), \min\{z(t) + r_i(\dot{z}(t)), \xi_i(t_{j-1})\}\}, \quad (3)$$

where  $x_i$  represent the initial conditions for memory of the rate-dependent play operator and can be considered as  $x_i = 0$ . The output of the RDPI model can be then expressed as a summation of weighted rate-dependent play operators as [22]

$$\Gamma[z](t) := \rho_0 z(t) + \sum_{i=1}^n \rho_i \Phi_{r_i(\dot{z}(t))}[z](t) \quad (4)$$

where  $\rho_0$  and  $\rho_i$  are the weights. The formulation of a linear rate-dependent threshold function yields a RDPI model that exhibits a linear increase in the magnitude of hysteresis with the excitation frequency of the input. The following rate-dependent threshold function has been selected

$$r_i(\dot{z}(t)) := \delta_1 i + \delta_2 |\dot{z}(t)|, \quad (5)$$

where  $\delta_1$  and  $\delta_2$  are positive constants which can be estimated based on the experimental results. This rate-dependent threshold function has been suggested in different studies to formulate a RDPI model that can characterize the rate-dependent hysteresis nonlinearities of smart materials-based actuators [7, 22, 23, 32]. Since the study focuses on the hysteresis compensation in real-time systems, then it is essential to introduce the discrete form of the RDPI

model. Considering the sampling time  $T_s = t_k - t_{k-1}$ , where  $k = 1, \dots, K$ , where  $K \in \mathbb{N}$  is an integer. The output of the discrete RDPI model is expressed as

$$y(k) = \Gamma[z](k) = \rho_0 z(k) + \Omega[z](k), \quad (6)$$

where

$$\Omega[z](k) = \sum_{i=1}^n \rho_i \Phi_{r_i(v_z(k))}[z](k), \quad (7)$$

where  $v_z(k) = \frac{z(k) - z(k-1)}{T_s}$  is the rate of the applied input in the discrete time domain. Let

$$\tilde{\xi}_i(k) = \Phi_{r_i(v_z(k))}[z](k)$$

where

$$\tilde{\xi}_i(k) = \max\{z(k) - r_i(v_z(k)), \min\{z(k) + r_i(v_z(k)), \tilde{\xi}_i(k-1)\}\}, \quad (8)$$

with

$$r_i(v_z(k)) = \delta_1 i + \delta_2 |v_z(k)|. \quad (9)$$

## 2.2 The Lipschitz continuity of the RDPI model

The proposed feedforward rate-dependent hysteresis compensator is a model-based feedforward controller constructed using the RDPI model. Then, it is essential to investigate the Lipschitz continuity property of the RDPI model in (6). (i) For  $k > 1$ , when the input  $z(k)$  increases, the output of the RDPI model is

$$y(k) = \rho_0 z(k) + \sum_{i=1}^n \rho_i (z(k) - r_i(v_z(k))), \quad \text{for } z(k) > z(k-1). \quad (10)$$

Since  $r_i(v_z(k)) > 0$  and  $\sum_{i=1}^n \rho_i > 0$ , the output when the input increases,  $z(k) > z(k-1)$ , can be expressed as

$$y(k) = \rho_0 z(k) + \sum_{i=1}^n \rho_i (z(k) - \delta_1 i - \delta_2 v_z(k)), \quad \text{for } z(k) > z(k-1). \quad (11)$$

Let  $\sigma_1(k) = z(k) - z(k-1)$  and  $\sigma_2(k) = z(k-1) - z(k-2)$ . Then

$$y(k) - y(k-1) = \sum_{i=0}^n \rho_i \left( \sigma_1(k) + \frac{\delta_2 (\sigma_2(k) - \sigma_1(k))}{T_s} \right). \quad (12)$$

If  $\sigma_1(k) > \sigma_2(k)$ , we have

$$y(k) - y(k-1) < (z(k) - z(k-1)) \sum_{i=0}^n \rho_i. \quad (13)$$

If  $\sigma_1(k) < \sigma_2(k)$ , then  $-\sigma_1(k) < 0 < \sigma_2(k) - \sigma_1(k)$ , hence

$$y(k) - y(k-1) > -(z(k) - z(k-1)) \sum_{i=0}^n \left( \rho_i - \frac{\delta_2}{T_s} \right) > -(z(k) - z(k-1)) \sum_{i=0}^n \rho_i. \quad (14)$$

From (13) and (14), we have

$$\left| y(k) - y(k-1) \right| < \left| z(k) - z(k-1) \right| \sum_{i=0}^n \rho_i, \quad \text{for } z(k) > z(k-1). \quad (15)$$

(ii) For  $k > 0$ , when the input  $z(k)$  decreases,  $z(k) < z(k-1)$ , we have

$$y(k) = \rho_0 z(k) + \sum_{i=1}^n \rho_i \left( z(k) + r_i(v_z(k)) \right), \quad \text{for } z(k) < z(k-1). \quad (16)$$

Then

$$y(k) = \rho_0 z(k) + \sum_{i=1}^n \rho_i \left( z(k) + \delta_1 i + \delta_2 v_z(k) \right), \quad \text{for } z(k) < z(k-1). \quad (17)$$

Thus

$$y(k) - y(k-1) = \sum_{i=0}^n \rho_i \left( \sigma_1(k) + \frac{\delta_2(\sigma_1(k) - \sigma_2(k))}{T_s} \right). \quad (18)$$

Following the same procedure as in (i), we conclude

$$\left| y(k) - y(k-1) \right| < \left| z(k) - z(k-1) \right| \sum_{i=0}^n \rho_i. \quad \text{for } z(k) < z(k-1). \quad (19)$$

(iii) When there is no increasing or decreasing  $z(k) = z(k-1)$ , we have  $y(k) = y(k-1)$ . For the RDPI model, we conclude

$$y(k) - y(k-1) \leq \left( z(k) - z(k-1) \right) \sum_{i=0}^n \rho_i. \quad (20)$$

Equation (20) reveals that the change in the output relies on both the weighting constants  $\sum_{i=0}^n \rho_i$ . Consequently,  $\sum_{i=0}^n \rho_i$  and the dynamic thresholds  $r_i(v_z(k))$  should be bounded and positive. This result is useful for the boundedness of the compensation error in the next section.

### 3 Inversion-Free Feedforward Rate-Dependent Hysteresis Compensation

The development of the proposed compensator is presented in this section with boundedness of the compensation error when the proposed model is applied for compensation of hysteresis nonlinearities. In addition, the section includes the parameters uncertainty of the RDPI model when the proposed compensator is applied.

### 3.1 The proposed compensator and the compensation error

Restructuring the RDPI model using inverse multiplicative scheme yields the rate-dependent hysteresis compensator. It is clear that the RDPI model includes linear reversible term  $\rho_0 z(k)$  and nonlinear hysteretic term  $\Omega(z)$ . Then, we can write  $\rho_0^{-1}(y(k) - \Omega[z](k)) = z(k)$ . In order to obtain a closed-form output in the real-time system, we consider  $\rho_0^{-1}(y(k) - \Omega[z](k-1)) = z(k)$ . Then, if we consider the reference input  $y_r(k)$ , the proposed inversion-free compensator is

$$z(k) = \rho_0^{-1}\left(y_r(k) - \Omega[z](k-1)\right). \quad (21)$$

To demonstrate that (21) can be used as a compensator, we will evaluate in the next subsection the compensation error. We will demonstrate that this error is bounded under certain condition on the employed sampling time  $T_s$ .

### 3.2 Evaluation of the compensation error and related condition

To evaluate the compensation error, the suggested rate-dependent compensator is applied as an input to the discrete representation of model in (6) as

$$y(k) = \Gamma\left[\rho_0^{-1}\left(y_r(k) - \Omega[z](k-1)\right)\right](k). \quad (22)$$

Let

$$\eta(k) = y_r(k) - \Omega[z](k-1). \quad (23)$$

Consequently, (22) can be expressed as

$$y(k) = \rho_0\left[\rho_0^{-1}\left(\eta(k)\right)\right] + \Omega\left[\rho_0^{-1}\left(\eta(k)\right)\right] \quad (24)$$

and

$$y(k) = y_r(k) + \Omega[z](k) - \Omega[z](k-1). \quad (25)$$

Hence, the error of the hysteresis compensation with the proposed compensator (21) is

$$e(k) = y(k) - y_r(k). \quad (26)$$

Let

$$y(k) = \rho_0 z(k) + \sum_{i=1}^n \rho_i \xi_i(k) \quad (27)$$

then, the compensation error can be expressed as

$$|e(k)| = |y(k) - y_r(k)|. \quad (28)$$

Using Equations (6) and (27), we have

$$|e(k)| = \left| \sum_{i=1}^n \rho_i (\xi_i(k) - \tilde{\xi}_i(k)) \right| \leq \sum_{i=1}^n \rho_i |\xi_i(k) - \tilde{\xi}_i(k)|. \quad (29)$$

To find an upper bound in (29), first, we prove the following result.

**Lemma 3.1** (*[33]*) *For any  $A, B, C, D \in \mathbb{R}$ , the following holds*

- (i)  $|\max\{A, B\} - \max\{C, D\}| \leq \max\{|A - C|, |B - D|\},$
- (ii)  $|\min\{A, B\} - \min\{C, D\}| \leq \max\{|A - C|, |B - D|\}.$

*Proof.* We prove (i) by considering four cases.

*Case 1:* If  $\max\{A, B\} = A$  and  $\max\{C, D\} = C$  then

$$|\max\{A, B\} - \max\{C, D\}| = |A - C| \leq \max\{|A - C|, |B - D|\}.$$

*Case 2:* If  $\max\{A, B\} = B$  and  $\max\{C, D\} = D$  then

$$|\max\{A, B\} - \max\{C, D\}| = |B - D| \leq \max\{|A - C|, |B - D|\}.$$

*Case 3:* If  $\max\{A, B\} = A$  and  $\max\{C, D\} = D$  then

$$|\max\{A, B\} - \max\{C, D\}| = |A - D| = \begin{cases} A - D \leq A - C & \text{if } A - D > 0 \\ D - A \geq C - A = -(A - C) & \text{if } A - D < 0. \end{cases}$$

Thus

$$|\max\{A, B\} - \max\{C, D\}| \leq |A - C| \leq \max\{|A - C|, |B - D|\}.$$

*Case 4:* If  $\max\{A, B\} = B$  and  $\max\{C, D\} = C$  then

$$|\max\{A, B\} - \max\{C, D\}| = |B - C| = \begin{cases} B - C \leq B - D & \text{if } B - C > 0 \\ C - B \geq D - B = -(B - D) & \text{if } B - C < 0. \end{cases}$$

Thus

$$|\max\{A, B\} - \max\{C, D\}| \leq \max\{|A - C|, |B - D|\}.$$

Same procedure can be used to prove (ii). ■

It follows from (29) and Lemma 3.1 that

$$\begin{aligned}
e(k) &\leq \sum_{i=1}^n \rho_i \max \{ |r_i(v_z(k)) - r_i(\dot{z}(k))|, \\
&\quad \left| \min \{ z(k) + r_i(\dot{z}(k)), \xi_i(k-1) \} - \min \{ z(k) + r_i(v_z(k)), \tilde{\xi}_i(k-1) \} \right| \} \\
&\leq \sum_{i=1}^n \rho_i \max \{ |r_i(v_z(k)) - r_i(\dot{z}(k))|, \\
&\quad \max \{ |r_i(\dot{z}(k)) - r_i(v_z(k))|, |\xi_i(k-1) - \tilde{\xi}_i(k-1)| \} \}. \tag{30}
\end{aligned}$$

Obviously, if

$$\max \left\{ |r_i(\dot{z}(k)) - r_i(v_z(k))|, |\xi_i(k-1) - \tilde{\xi}_i(k-1)| \right\} = |r_i(\dot{z}(k)) - r_i(v_z(k))|,$$

then

$$e(k) \leq \sum_{i=1}^n \rho_i |r_i(v_z(k)) - r_i(\dot{z}(k))|.$$

Using Backward Euler scheme in  $v_z(k)$ , we have

$$|\dot{z}(k) - v_z(k)| \leq M_k T_s$$

where  $M_k$  is a positive number. Thus

$$\sum_{k=1}^K |\dot{z}(k) - v_z(k)| \leq K M_k T_s.$$

When a sufficient small  $T_s$  is selected such that  $K M_k T_s < \zeta$  for some small positive number  $\zeta$ . Let  $\varepsilon_i > 0$ , since  $r_i$  are considered as absolutely continuous functions, we have

$$\sum_{k=1}^K |r_i(\dot{z}(k)) - r_i(v_z(k))| < \varepsilon_i$$

whenever

$$\sum_{k=1}^K |\dot{z}(k) - v_z(k)| < \zeta.$$

Hence, for each  $k \in \{1, \dots, K\}$

$$|r_i(\dot{z}(k)) - r_i(v_z(k))| < \varepsilon_i.$$

Let  $\varepsilon = \max \{\varepsilon_i\}$ . Then,

$$\sum_{i=1}^n |r_i(\dot{z}(k)) - r_i(v_z(k))| < n\varepsilon.$$

This yields

$$e(k) < n^2 \rho_{\max} \varepsilon, \tag{31}$$

where  $\rho_{\max} = \max \{\rho_i\}$ . The bound of the error is  $\mathcal{E} = n^2 \rho_{\max} \varepsilon$ . For very small value of  $\varepsilon$ , the suggested compensator would yield

$$y(k) \cong y_r(k). \tag{32}$$

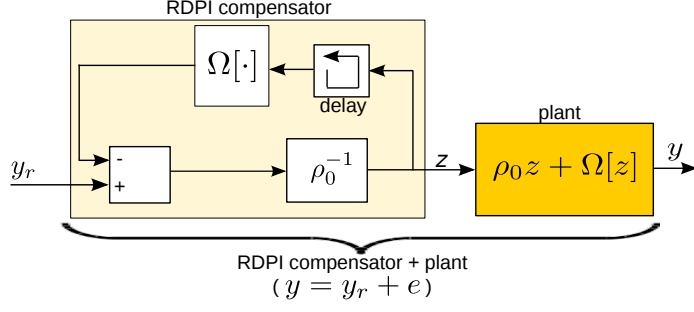


Fig. 1. Block diagram of the RDPI compensator based on inverse multiplicative structure and of the hysteretic plant.

When

$$\max \left\{ |r_i(\dot{z}(k)) - r_i(v_z(k))|, |\xi_i(k-1) - \tilde{\xi}_i(k-1)| \right\} = |\xi_i(k-1) - \tilde{\xi}_i(k-1)|,$$

same procedure as above can be carried out. Consequently,  $y(k) \cong y_r(k)$ . Hence, the suggested rate-dependent hysteresis compensator guarantees the tracking performance of a hysteretic plant that exhibits rate-dependent hysteresis nonlinearities. The following condition is suggested to obtain low compensation error

$$T_s < \frac{1}{(n\rho_0 + 1)(n\rho_{\max}i + 1)(f_{\max} + 1)}. \quad (33)$$

Figure 1 depicts the block diagram of the proposed rate-dependent hysteresis compensation methodology. As the figure illustrates, the hysteresis compensator is formed by restructuring the RDPI model itself using inverse multiplicative scheme. The delay block in the figure represents a one sampling time  $T_s$  delay.

### 3.3 Discussions

The previous analysis shows that restructuring the RDPI model in (6) contributes a rate-dependent compensator that can be employed for compensation of the rate-dependent hysteresis nonlinearities of the model. Consequently, the extra calculations to formulate the inverse model are not required. In addition, the conditions that have to be satisfied to obtain an analytical inverse model can be ignored. The proposed compensator can also be employed to cancel out the rate-independent hysteresis nonlinearities observed at shallow levels of input frequency, i.e., for  $r_i(v_z(k)) = \delta_1 i$  (for thresholds independent from the rate/frequency of the input). It can be concluded that when the control

signal increases,  $z(k) > z(k-1)$ , the error can be expressed as

$$|e_{\text{ind}}(k)| \leq \sum_{i=1}^n \rho_i \max\{|\Delta z(k)|, |\Delta \xi_i(k)|\}, \quad (34)$$

where  $\Delta z(k) = z(k) - z(k-1)$ ,  $\Delta \xi_i(k) = \xi_i(k) - \xi_i(k-1)$  and

$$|e_{\text{ind}}(k)| \leq n\rho_{\max}\mathcal{E}. \quad (35)$$

From (31) and (32), the output of the hysteresis compensation can be represented using a linear  $y_r(k)$  and a nonlinear bounded terms  $e(k)$ :

$$y(t) = y_r(k) + e(k). \quad (36)$$

Consequently, feedforward-feedback control architecture such as  $H_\infty$  control [34–36], sliding mode [37], adaptive [38] and PID structured controllers [39] techniques can be applied with the formula (36).

### 3.4 Parameters uncertainty

This section investigates the parameters uncertainty of the RDPI model when the proposed compensator is applied for compensation of hysteresis nonlinearities. Let us write the output of the estimated discrete RDPI model is assumed to be slightly different to the real model in (6)

$$\hat{y}(k) = \hat{\Gamma}[z](k) := \hat{\rho}_0 z(k) + \hat{\Omega}[z](k), \quad (37)$$

where  $\hat{\rho}_0$  is a positive constant and

$$\hat{\Omega}[z](k) = \sum_{i=1}^n \hat{\rho}_i \Phi_{\hat{r}_i(v_z(k))}[z](k), \quad (38)$$

where  $\hat{\rho}_i$  are positive constants. The proposed compensator constructed with the estimated RDPI model is

$$z(k) = \hat{\rho}_0^{-1} \left( y_r(k) - \hat{\Omega}[z](k-1) \right). \quad (39)$$

Then, when applying the compensator (39) calculated from the estimate model (37) to the real model (6), we have the output of the compensation as follows

$$y(k) = \rho_0 \hat{\rho}_0^{-1} y_r(k) - \rho_0 \hat{\rho}_0^{-1} \hat{\Omega}[z](k-1) + \Omega[z](k) \quad (40)$$

and the error is

$$e(k) = y_r(k)(1 - \rho_0 \hat{\rho}_0^{-1}) + \rho_0 \hat{\rho}_0^{-1} \hat{\Omega}[z](k-1) - \Omega[z](k). \quad (41)$$

Let  $\rho_0 \hat{\rho}_0^{-1} = \tau$  and

$$\mathcal{P}[k] = \rho_0 \hat{\rho}_0^{-1} \hat{\Omega}[z](k-1) - \Omega[z](k),$$

then

$$\mathcal{P}[k] = \sum_{i=1}^n \left( \tau \hat{\rho}_i \Phi_{r_i(v_z(k-1))}[z](k-1) - \rho_i \Phi_{r_i(v_z(k))}[z](k) \right) \quad (42)$$

and

$$\begin{aligned} \mathcal{P}[k] = \sum_{i=1}^n \max\{ & |\tau \hat{\rho}_i z(k-1) - \rho_i z(k) \\ & + \tau \hat{\rho}_i r_i(v_z(k-1)) - \rho_i r_i(v_z(k))|, |\xi_i(k) - \xi_i(k-1)|\}. \end{aligned} \quad (43)$$

For  $\hat{\rho}_i = \rho_i + \lambda_i$ , we have

$$\begin{aligned} \mathcal{P}[k] = \sum_{i=1}^n \max\{ & |(\tau \rho_i + \tau \lambda_i) z(k-1) - \rho_i z(k) + (\tau \rho_i \\ & + \tau \lambda_i) r_i(v_z(k-1)) - \rho_i r_i(v_z(k))|, |\xi_i(k) - \xi_i(k-1)|\} \end{aligned} \quad (44)$$

and

$$\begin{aligned} |\mathcal{P}[k]| \leq \sum_{i=1}^n \max\{ & |\tau \rho_i z(k-1) - \rho_i z(k) + \tau \rho_i r_i(v_z(k-1)) - \rho_i r_i(v_z(k))| \\ & + \tau \lambda_i z(k-1) + \tau \lambda_i r_i(v_z(k-1)), |\xi_i(k) - \xi_i(k-1)|\}. \end{aligned} \quad (45)$$

Let  $\max\{|\tau z(k) - z(k-1)|\} = \bar{\epsilon}_1$ ,  $\max\{|z(k-1) + r_i(v_z(k-1))|\} = \kappa$ ,  $\max\{|\tau r_i(z(k-1)) - r_i(z(k))|\} = \bar{\epsilon}_2$ , and  $\lambda_{\max} = \max\{|\lambda_i|\}$ , where  $\bar{\epsilon}_1$ ,  $\bar{\epsilon}_2$ , and  $\kappa$  are positive constants. Then the error is

$$|e(k)| \leq |y_r(k)(1 - \tau)| + n \rho_{\max} \{\bar{\epsilon}_1 + \bar{\epsilon}_2 + \lambda_{\max} \kappa, \mathcal{E}\}. \quad (46)$$

Thus

$$|e(k)| \leq |y_r(k)|(1 - \tau) + n \rho_{\max} \{\bar{\epsilon}_1 + \bar{\epsilon}_2 + \lambda_{\max} \kappa, \mathcal{E}\}. \quad (47)$$

It can be concluded that the tracking error is still bounded when the uncertainties of the RDPI model parameters are considered for compensation of hysteresis nonlinearities.

## 4 Application to a piezoelectric cantilever actuator

In this section, the suggested feedforward rate-dependent compensator is applied for compensation of rate-dependent hysteresis nonlinearities of piezoelectric cantilever actuator. This actuator exhibits rate-dependent hysteresis nonlinearities under harmonic excitations and oscillations in the output displacement when subjected to step inputs. Piezoelectric cantilever actuators are considered attractive for micro-assembly and can be used as micro-grippers for manipulating small objects at micro level [3, 30, 31, 40, 41].

### 4.1 The experimental platform

The piezoelectric cantilever actuator is depicted in Figure 2 within a simple schematic representation of the experimental platform. The Figure shows a 2-DOF piezoelectric cantilever actuator of  $25\text{mm}$  length and  $1\text{mm} \times 1\text{mm}$  cross section. The actuator exhibits the output displacement (deflection)  $y[\mu\text{m}]$  when subjected to input voltage  $z[\text{V}]$ . The actuator was fabricated to move in two different axes. However, only the motion in  $Y$ -axis was considered in the experimental study. The maximal operating range of input voltage that can be applied to the actuator is  $\pm 10\text{V}$ . An inductive position sensor was used to capture the output displacement of the actuator. The sensor is used: i) to characterize the actuator's hysteresis, creep and step responses, ii) to verify the performances obtained with the RDPI hysteresis compensator, iii) and to make a feedback signal for a further feedback controller. The sensor has a bandwidth of  $5\text{kHz}$  and resolution down to  $10\text{nm}$ . A computer equipped with a dSPACE acquisition system of  $T_s = 50\mu\text{s}$  sampling time is used for generating the excitation input voltage and acquiring the measured output displacement.

### 4.2 Actuator characterization

In order to characterize the piezoelectric actuator, first we apply a sinusoidal input (driving) voltage. Its amplitude is of  $8\text{V}$  and different excitation frequencies have been used:  $1\text{Hz}$  to  $100\text{Hz}$ . Figure 3 shows the obtained displacement

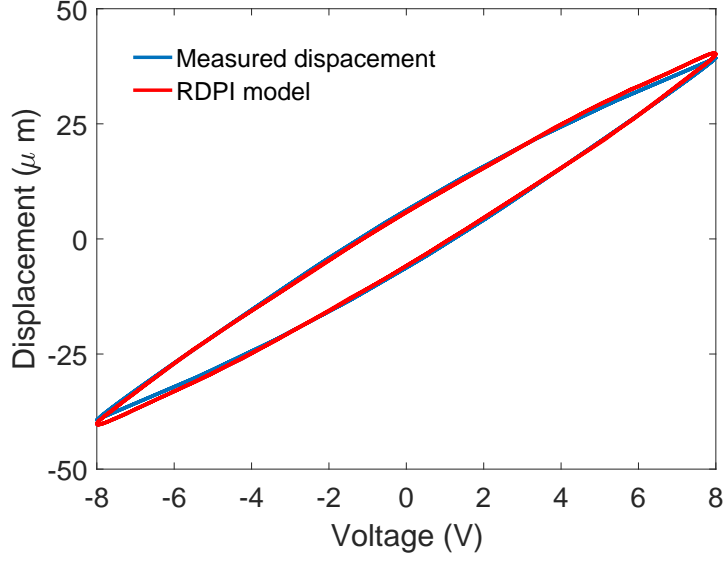


Fig. 2. 2-DOF piezoelectric cantilever and schematic representation of the experimental platform.

versus the input voltage for three frequencies:  $1Hz$ ,  $50Hz$ , and  $100Hz$ . Beyond the hysteresis nonlinearity property and the fact that its shape changes versus the frequency (rate-dependency), it shows that the range of displacement is of about  $\pm 40\mu m$  for a voltage of  $\pm 8V$ , i.e. the gain is:  $5[\frac{\mu m}{V}]$ . Such gain is very interesting in piezoelectric actuator based on cantilever structure and devoted to micromanipulation task.

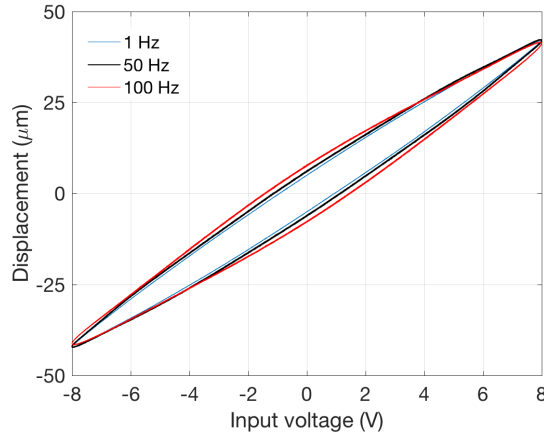


Fig. 3. Measured hysteresis loops of the piezoelectric cantilever actuator under a sinusoidal voltage with  $8V$  of amplitude and  $1Hz$ ,  $50Hz$ , and  $100Hz$  of excitation frequency.

Then, we apply a step input voltage of  $8V$  to the actuator. The response is depicted in in [Figure 4](#) which clearly show the badly damped oscillations property of the actuator. A quick identification shows that the first resonant frequency is of  $1.627kHz$ .

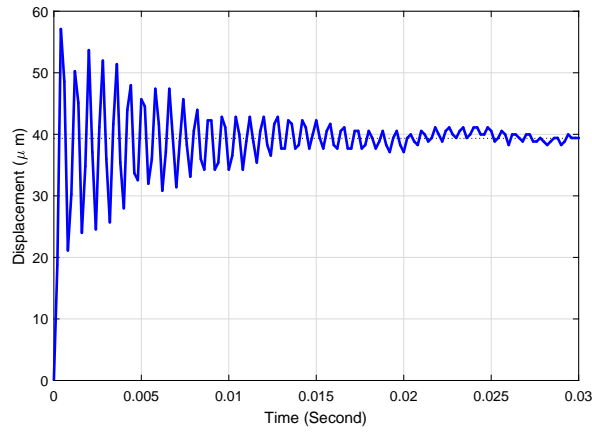


Fig. 4. Step response of the actuator with 8V of input voltage.

Finally, we still measure the step response of the actuator but, rather than measuring for 30ms (see Figure 4), we measure for a long duration period (several tens of seconds). The response is shown in Figure 5 where we see that, just after the transitory part characterized above, there is a low rate drift. This drift is called creep phenomenon and is typical for piezoelectric actuator. Similarly to hysteresis, the creep phenomenon introduces precision loss in the tasks to be carried out and should therefore be controlled. In this paper, the hysteresis will be controlled in a feedforward manner and the creep will be considered as additional error that will be considered in the feedback controller.

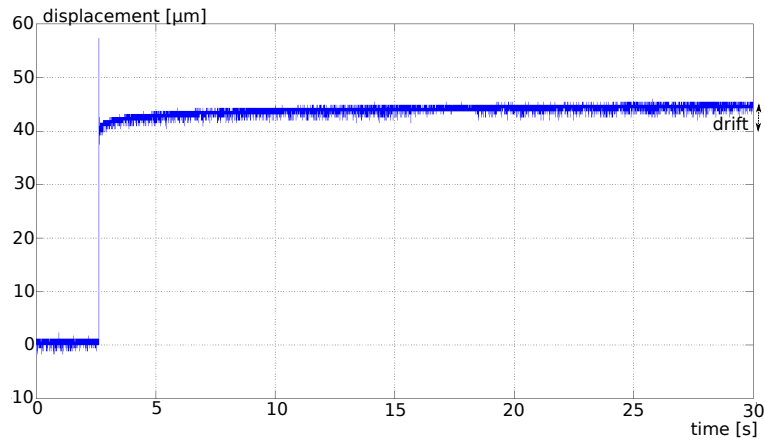


Fig. 5. Creep phenomenon observed in the step response during a long duration period.

### 4.3 Hysteresis modeling and parameters identification

The formulation of the rate-dependent hysteresis compensator that can compensate for the hysteresis nonlinearity of the piezoelectric actuator necessitates formulating a rate-dependent model. We use therefore the RDPI model described in Section II. The measured data that are illustrated in [Figure 3](#) can be employed to identify the parameters of the RDPI model. The characterization error can be defined as

$$e_c(k) = \Gamma[z](k) - y(k), \quad (48)$$

where  $y(k)$  represents the measured displacement of the piezoelectric cantilever actuator when an input voltage  $z(k)$  at a particular excitation frequency is applied, and  $\Gamma[z](k)$  is the output of the RDPI model with  $z(k)$ . The index  $k$  ( $k = 1, 2, \dots, K$ ) refers to the number of data points considered in computing the error for one complete hysteresis loop. The parameter vector  $\Pi = \{\delta_1, \delta_2, \rho_0, \rho_1, \rho_2, \dots, \rho_{10}\}$  of the RDPI model  $\Gamma$  is identified through solving the least-square problem of the characterization error function in (48) over different excitation frequencies as

$$\min \left( \sum_{k=0}^K e_c^2(k) \right) = \min \left( \sum_{k=0}^K (\Gamma[z](k) - y(k))^2 \right), \quad (49)$$

where  $\Gamma[z](k)$  is the response of the discrete RDPI model in (6).

The MATLAB constrained optimization toolbox subjected to  $\delta_1 > 0$  and  $\delta_2 > 0$  constrains is used to estimate the parameters. The number  $n$  has been chosen as  $n = 10$ . The identified parameters of the model are:  $\delta_1 = 1.0136$ ,  $\delta_2 = 3.9486 \times 10^{-4}$ ,  $\rho_0 = 0.6214$ ,  $\rho_1 = 0.1351$ ,  $\rho_2 = 0.1079$ ,  $\rho_3 = 0.0862$ ,  $\rho_4 = 0.0689$ ,  $\rho_5 = 0.0550$ ,  $\rho_6 = 0.0439$ ,  $\rho_7 = 0.0351$ ,  $\rho_8 = 0.0280$ , and  $\rho_9 = 0.0224$ , and  $\rho_{10} = 0.0179$ . [Figure 6-a, b and c](#) depict the model simulation plotted with the experimental result for different frequencies ( $1Hz$ ,  $50Hz$  and  $100Hz$ ) which show the good convenience of the identified model. Furthermore, the maximum percentage characterization errors are presented in [Figure 6-d](#) with more frequencies between  $1Hz$  and  $100Hz$  band which confirms that the error of tracking is less than 3%.

### 4.4 Linear dynamics modeling

Beside the rate-dependent hysteresis nonlinearity, the piezoelectric cantilever actuator exhibits a high dynamics under step inputs. Consider the scheme in

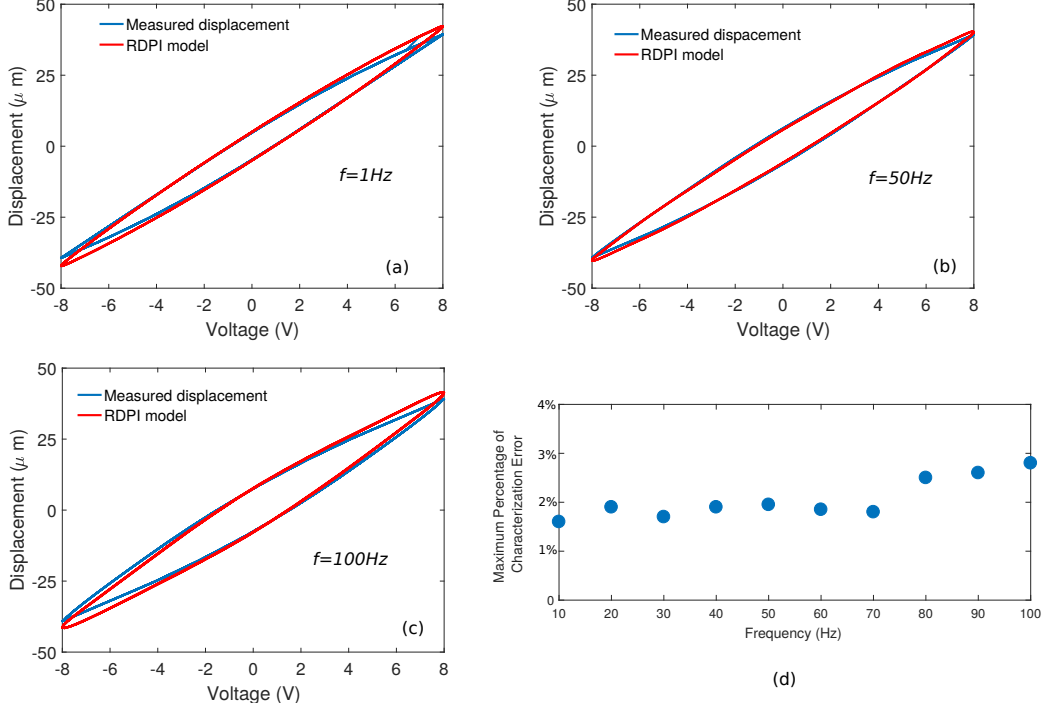


Fig. 6. Comparison between the measured hysteresis loops and the output of the RDPI model at  $1\text{Hz}$  (a),  $50\text{Hz}$  (b), and  $100\text{Hz}$  (c). (d): The characterization error maximum percentage of the RDPI model.

Figure 7-a to represent the plant with its dynamics. It is composed of the RD hysteresis model and a linear dynamics related to the mechanical part. In the literature, it is usual to use a rate-independent hysteresis followed by a linear dynamics for piezoelectric actuators. In our case, rather than using a rate-independent hysteresis, we use rate-dependent (RD) which permits more model precision. Thus, the RD hysteresis model can be modeled and identified with a RDPI of the previous sections and the approximate model  $\hat{G}(s)$  of the real dynamics  $G(s)$  (see Figure 7-b) can be identified by using the step response in Figure 4.

The step input voltage of  $A\gamma[V]$  is applied to the piezoelectric cantilever, where  $A$  is the desired step input voltage and  $\gamma$  is a constant used to eliminate the effects of the rate-dependent hysteresis nonlinearities. The output of the model considering the increasing output of the model with  $u(t) = A\gamma$  and  $r_i(\dot{z}(t)) = \sigma_i$  is:

$$\Gamma[A\gamma] = \rho_0 A\gamma + \sum_{i=1}^n \rho_i \Phi_{\sigma_i} [A\gamma] \quad (50)$$

and

$$\Gamma[A\gamma] = \rho_0 A\gamma + \sum_{i=1}^n \rho_i (A\gamma - r_i) \quad (51)$$

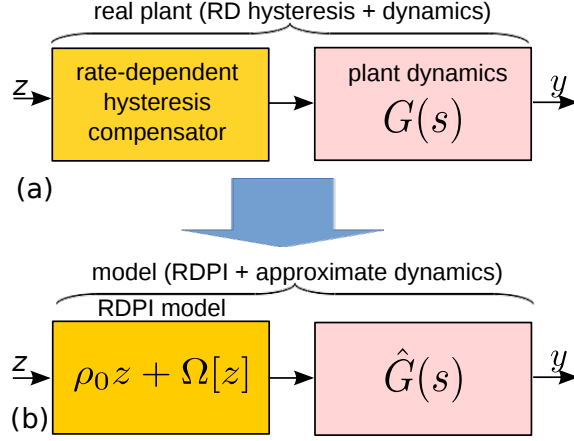


Fig. 7. Block diagram of the plant with its dynamics.

and  $\Gamma[A\gamma] = \sum_{i=0}^n \rho_i A\gamma - \sum_{i=1}^n \rho_i r_i$ . Then to obtain  $\Gamma[A\gamma] = A$ , we have

$$\gamma = \frac{A + \sum_{i=1}^n \rho_i r_i}{A \sum_{i=0}^n \rho_i}. \quad (52)$$

For  $A = 8V$ ,  $\sum_{i=0}^n \rho_i = 1.614$ ,  $\sum_{i=1}^n \rho_i r_i = 2.3047$ , and  $\gamma = 1.0558$ . Then, in order to eliminate the hysteresis effects from the response of the actuator when the step input voltage  $8V$  is applied, we consider the gain of  $1.0558$  to obtain the output of the linear dynamics only. Figure 8 shows the simulation results.

The identification of  $\hat{G}(s)$  has been carried out with a Box-Jenkins parameters identification technique with different orders and with standard deviation which indicates the model precision for each suggested order. It is shown that beyond an order of 4, the standard deviation stops decreasing substantially. We therefore choose the following fourth order model

$$\hat{G}(s) = \frac{10854(s + 1146)(s^2 - 1452s + 2.7e8)}{(s + 9200)(s + 1095)(s^2 + 312s + 6.7e7)}, \quad (53)$$

where  $e\theta$  denotes  $\times 10^\theta$ , for instance  $2.7e8 = 2.7 \times 10^8$ . Figure 9 presents a comparison between the step response of the actuator and  $\hat{G}(s)$  under  $8V$  input voltage and shows a good convenience between them.

#### 4.5 Compensation of the rate-dependent hysteresis of the actuator

The identified RDPI model is restructured to obtain the corresponding inverse multiplicative scheme as illustrated in Figure 1. The effectiveness of the proposed compensator was subsequently examined at different excitation

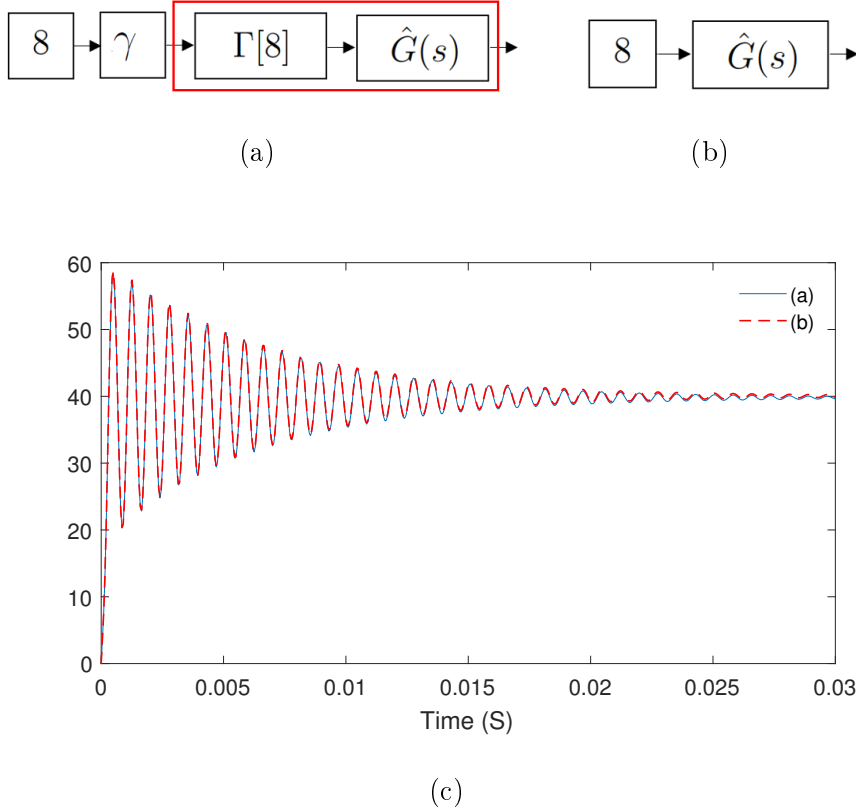


Fig. 8. Block diagram of the plant with its dynamics when the step input voltage of  $8V$ .

frequencies. The output displacement of the actuator when the proposed rate-dependent compensator is applied as a feedforward compensator are given in [Figure 10](#). The figure shows the output displacement  $y[\mu m]$  versus the desired displacement  $y_r[\mu m]$  at different excitations of input frequency:  $1Hz$ ,  $50Hz$  and  $100Hz$ . The compensation results demonstrate that the proposed compensator can indeed reduce the rate-dependent hysteresis of the actuator. However, the results reveal slight compensation errors at high excitations of input frequency.

In order to verify the efficiency of the RDPI compensation to handle minor loops as well as biased minor loops, we compare the hysteresis with and without the suggested compensator. For that, we apply the following driving voltage to the actuator (without compensator):  $z(t) = 3V \sin(2 \times \pi \times 8Hz \times t) + 8V \sin(2 \times \pi \times 1Hz \times t)$ , where  $t = kT_s$ . The time-domain output displacement  $y$  is displayed in [Figure 11-a](#): the experimental result and the RDPI model simulation. The related hysteresis is displayed in [Figure 11-b](#) in which we can observe biased and unbiased minor loops. After implementing the compensator, a desired displacement  $y_r$  with the same shape than above  $z$  has been

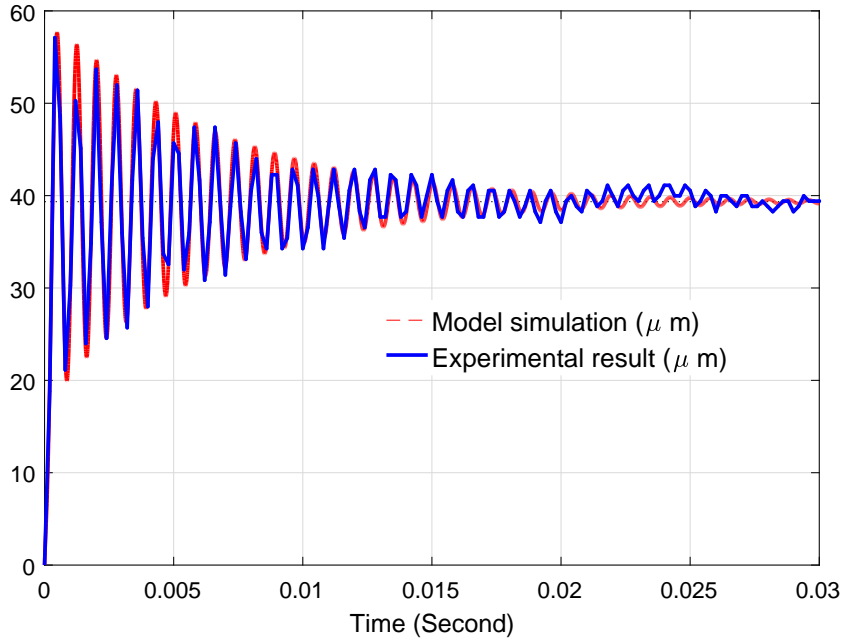


Fig. 9. A comparison between the step response of the piezoelectric actuator and the identified linear dynamics model  $\hat{G}(s)$ .

applied in order to have similar minor loops. Figure 11-c provides the input-output map  $(y_r, y)$  where we observe that the hysteresis even for biased minor loops have been removed.

The RDPI compensator does not account for the creep. Indeed, for this actuator, the creep phenomenon acts at very low frequency (much lower than  $1Hz$ ), whilst the RDPI model and thus the compensator has been identified from  $1Hz$ . Two ways are possible to compensate for the creep phenomenon additionally to the hysteresis: i) identifying the RDPI model and compensator from very low frequency (much less than  $1Hz$ ), ii) or cascading a creep compensator [42] with the actual RDPI compensator. However, since we further add an internal model-based feedback controller, the creep phenomenon can comfortably be considered as additional error that will be rejected by this latter, like the compensation error and like eventual external disturbance.

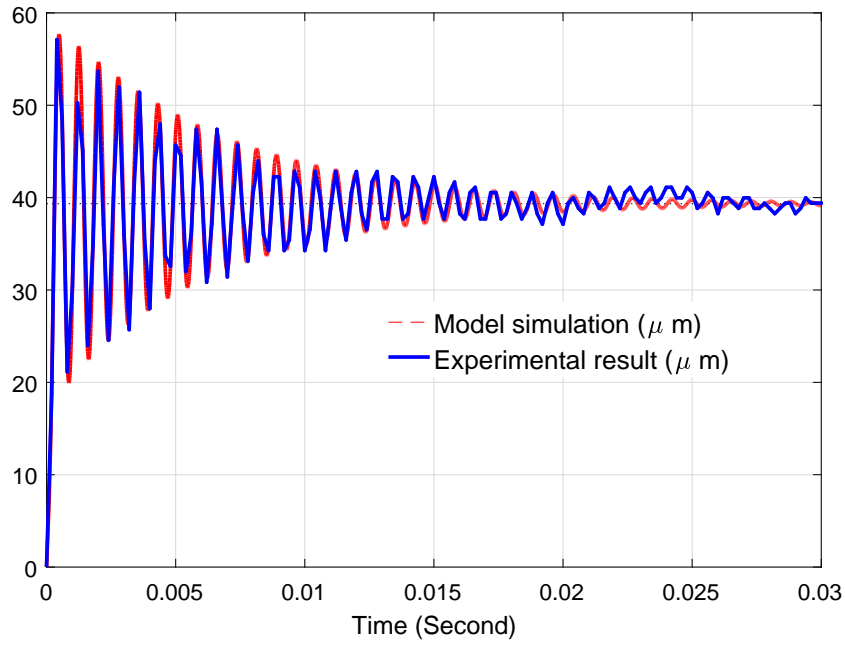


Fig. 10. Input-output map of the piezoelectric actuator when the proposed compensator is applied in a open-loop manner at excitation frequency of  $1Hz$  (a),  $50Hz$  (b) and  $100Hz$  (c).

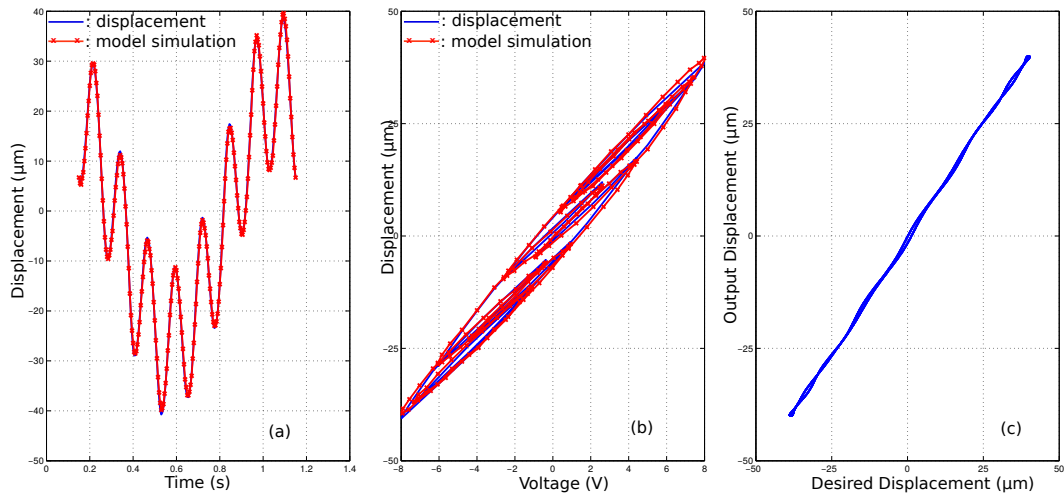


Fig. 11. Experimental tests with biased minor loops. (a): time-domain curves when without compensation. (b): hysteresis curves when without compensation. (c): hysteresis curves with compensation.

## 5 Internal model-based feedback control design for the piezoelectric cantilever actuator

Feedback control techniques can be used to enhance the performance of piezoelectric actuator under step and harmonic inputs. In this section, an internal model-based control architecture will be synthesized. The controller will be afterwards applied with the proposed hysteresis compensator to a piezoelectric cantilever actuator.

### 5.1 Synthesizing an internal model-based feedback controller

Control systems that integrate smart material-based actuators might experience internal or external perturbations that yield substantial errors and subsequently reduce the efficiency of the system in performing the desired tasks. Consequently, the compensation error  $e(k)$  in (36) can be assumed as an internal perturbation to the compensated system. Introducing the dynamics behavior in (53) and working back in the continuous domain, the static model of (36) becomes the following dynamic model:

$$y(s) = \hat{G}(s)y_r(s) + e(s). \quad (54)$$

The linear model with disturbance in (54), derived from the RDPI feedforward hysteresis compensation, is augmented in this section with a feedback controller that can enhance the tracking performance of the piezoelectric cantilever actuator under various conditions. Notice that additionally to the compensation error, eventual external disturbance could occur during a micromanipulation task, such as the manipulation force. Furthermore, the linear model  $\hat{G}(s)$  might be uncertain as we shown in section 3.4. This is particularly true if the actuator is intended to work in an environment where the ambient temperature varies, knowing that the hysteresis of cantilever structured piezoelectric actuators like the one in this papers are very sensitive to the environment [43, 44]. It is therefore essential to use a feedback controller that consider the error  $e(s)$ , eventual external disturbances and eventual model uncertainties. One of the techniques that could consider such specifications is the internal model control (IMC). In our case, its advantage over other robust techniques such as  $H_\infty$  is obvious: the controller is very simple to synthesize since it is based on the model and on a low order filter, as we will see.

The internal model-based feedback design is implemented as a feedback controller that permits the consideration of the external perturbation and addresses the modeling errors as well as model uncertainties. Let [Figure 12-a](#)

illustrate the suggested combination of the RDPI compensation (feedforward control) and of the internal model control (feedback control). The exogenous reference input signal in the figure is denoted by  $r_y$ ,  $C(s)$  is the feedback controller to be designed while  $\hat{G}(s)$  represents the approximate model of the dynamics that we have identified previously and that should be sufficiently close to the real dynamics  $G(s)$  of the piezoelectric cantilever actuator. In the ideal case where  $\hat{G}(s) = G(s)$  and the RDPI model exact matches the hysteresis, [Figure 12-a](#) would be similar to [Figure 12-b](#). Otherwise, considering that  $\hat{G}(s) \neq G(s)$  and the RDPI compensator has compensation error  $e(t)$ , [Figure 12-a](#) results in [Figure 12-c](#). In this, the internal disturbance  $e(s)$  rassembles the compensation error as described previously.

It is worth to note that the scheme in [Figure 12-a](#) is a combination of a (cascade) feedforward controller and of a feedback controller. Differently from feedforward plant-injection (FFPI) and from feedforward closed-loop injection (prefilter) combined with feedback, the cascade feedforward combined with feedback controller which is proposed in this paper permits to obtain a linear system with the compensator and then to use a linear feedback controller. Such architecture has been applied in various applications [\[5,45–48\]](#).

As [Figure 12](#) illustrates, we have

$$y = \frac{GC}{(1 + C(G - \hat{G}))} r_y + \frac{(1 - \hat{G}C)}{(1 + C(G - \hat{G}))} e \quad (55)$$

Selecting the controller

$$C(s) = \frac{1}{\hat{G}(s)} \quad (56)$$

will yield a zero steady-state error, and will completely reject the disturbance irrespective to a constant error  $e(t)$ , for any constant reference  $r_y(t)$  as well as any approximated model  $\hat{G}(s)$ . Although this choice can enhance the steady-state response, the transient response is ignored. In order to address the transient part with a desired settling time  $t_r$  in the output of the closed-loop system, the controller  $C(s)$  can be selected such that

$$C(s) = F(s) \frac{1}{\hat{G}(s)} \quad (57)$$

where

$$F(s) = \frac{1}{1 + \frac{t_r}{3}s}. \quad (58)$$

This filter is directly associated with the desired closed-loop response [\[49\]](#). It can be noted from the previous assumption that if the internal model  $\hat{G}(s)$  is

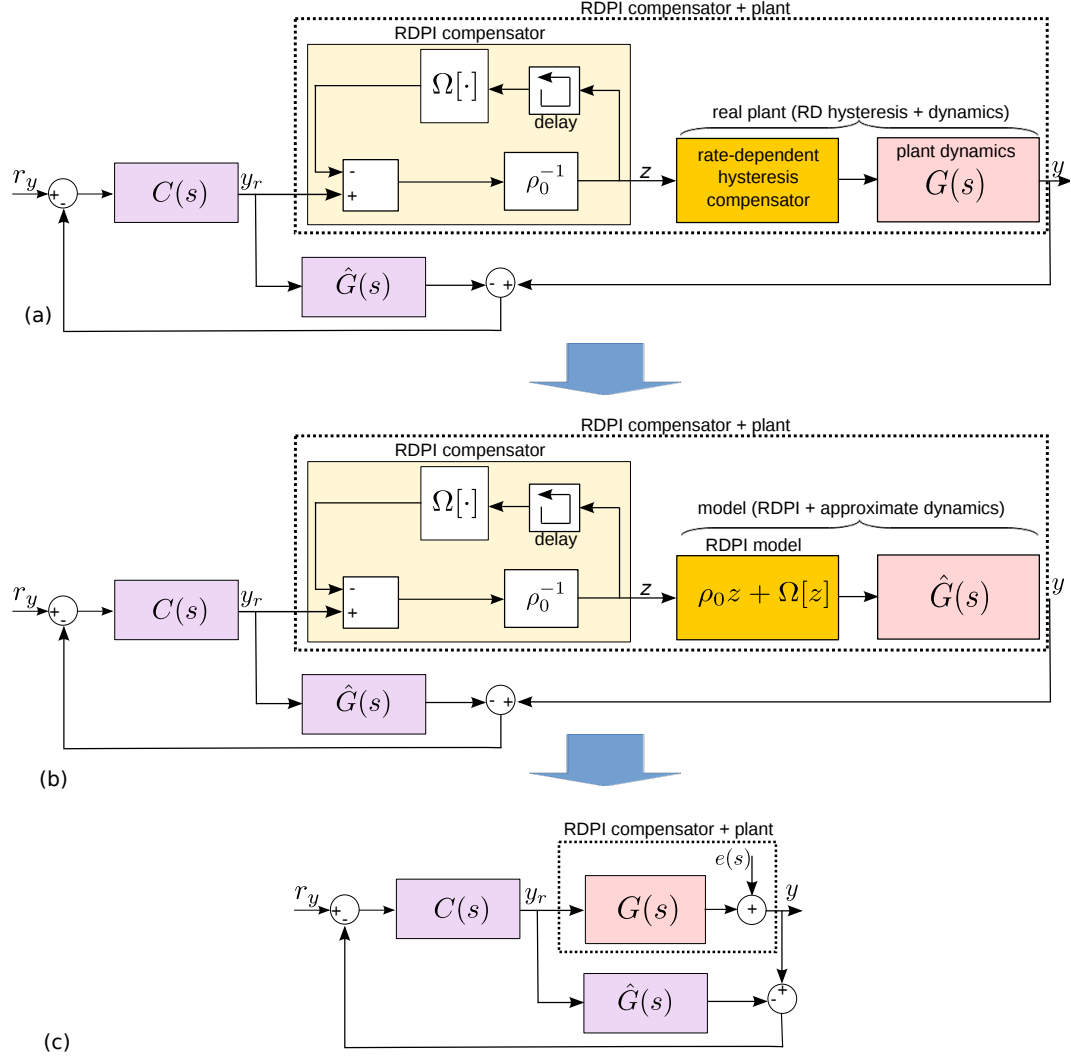


Fig. 12. (a): block-diagram of the feedforward-feedback control scheme. (b): block-diagram of the feedforward-feedback control scheme with model which exact matches with the real plant. (c): equivalent diagram.

exact ( $\hat{G}(s) = G(s)$ ), then

$$y(s) = F(s)r_y(s) + (1 - F(s))e(s). \quad (59)$$

Consequently, the desired transient part can be addressed, the zero steady-state error and the disturbance rejection requirements are fulfilled.

If the estimated linear dynamic model  $G(s)$  is not exact, then

$$y = \frac{\frac{G}{\hat{G}}F}{\left(1 + F\left(\frac{G}{\hat{G}} - 1\right)\right)}r_y + \frac{(1 - F)}{\left(1 + F\left(\frac{G}{\hat{G}} - 1\right)\right)}e. \quad (60)$$

In this case, both the zero steady-state and the disturbance rejection are still guaranteed. However, the transient part is ignored which is mostly attributed

to the difference with the desired transient part  $F(s)$ . This difference significantly increases if  $\hat{G}(s)$  has not been identified properly. It is worth to summarize that the compensation error and the creep phenomenon can be rassembled in the signal  $e(s)$  of [Figure 12](#) while the mdoel uncertainty is considered in the difference between  $\hat{G}(s)$  and  $G(s)$ .

## 5.2 Application of the internal model-based feedback control design to the piezoelectric actuator

After estimating the system  $\hat{G}(s)$  that can represent the real dynamic model  $G(s)$  of the compensated system, a desired feedback behavior  $F(s)$  has to be given. A transient response without overshoot and with a settling time of  $t_r = 10ms$  was considered as desired specifications for the closed-loop. These specifications were selected to obtain a better tracking compared to the response obtained from the initial system  $\hat{G}(s)$  (and  $G(s)$ ) in [Figure 9](#). Constructing  $F(s)$  based on desired requirements was employed to yield the controller  $C(s)$  such that  $C(s) = F(s)\frac{1}{\hat{G}(s)} = \frac{1}{(1+3.7\times 10^{-3}s)\hat{G}(s)}$ , where  $\hat{G}(s)$  is given by (53). As illustrated in the previous section the internal model-based feedback controller is composed of the controller  $C(s)$  and also the  $\hat{G}(s)$  which are placed in parallel with the compensated system as depicted in [Figure 12](#).

In order to examine the effectiveness of the proposed controller, a step input  $r_y$  was first applied to the compensated system augmented with the internal model closed-loop control, i.e. to the feedforward-feedback scheme. The measured output displacement of the actuator when the reference input  $r_y = 40\mu m$  is applied is shown in [Figure 13](#). As the figure illustrates, the desired specifications are fully respected: there is no overshoot and the badly damped oscillations in [Figure 4](#) are completely removed, while the settling time is found to be  $t_r \approx 10ms$ , see [Figure 13-a](#). Furthermore, when we observe the step response over a long period, we see that the drift due to the creep phenomenon in [Figure 5](#) is also completely removed.

The next experiment consists in applying a varying input reference displacement  $r_y$  to the feedforward-feedback scheme. The reference variation is generated by manually moving a slider in the software (*Controldesk*) that serves as graphical interface in the computer. The range of the reference is still limited within  $\pm 40\mu m$ , which is the range of characterization and identification. The response is given in [Figure 14-a](#) where we can see that the controlled actuator tracks successfully the desired displacement. [Figure 14-b](#) depicts the tracking error ( $r_y - y$ ) which remains around zero, except for some peaks that occur at the brusque change of the reference and despite the noise due

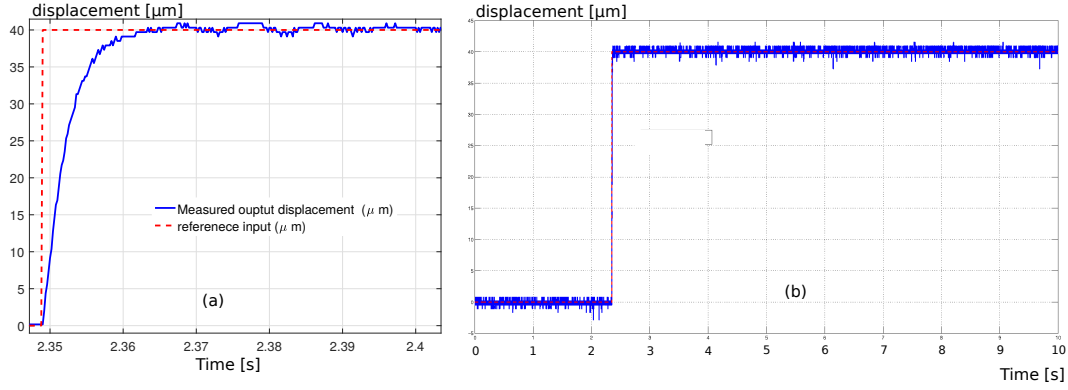


Fig. 13. Experimental step response of the closed-loop with the proposed feedforward-feedback control: (a) the transient part, (b) the response over a long period.

to the sensor. The root-mean-square value of the error has been calculated ( $RMS_{error} = \frac{1}{N_x} \sum_{k=1}^{N_x} (r_y(k) - y(k))^2$ ), where  $N_x$  is the number of experimental points. We obtained  $RMS_{error} = 0.2\mu m$  which is negligible relative to the range of displacement ( $\pm 40\mu m$ ).

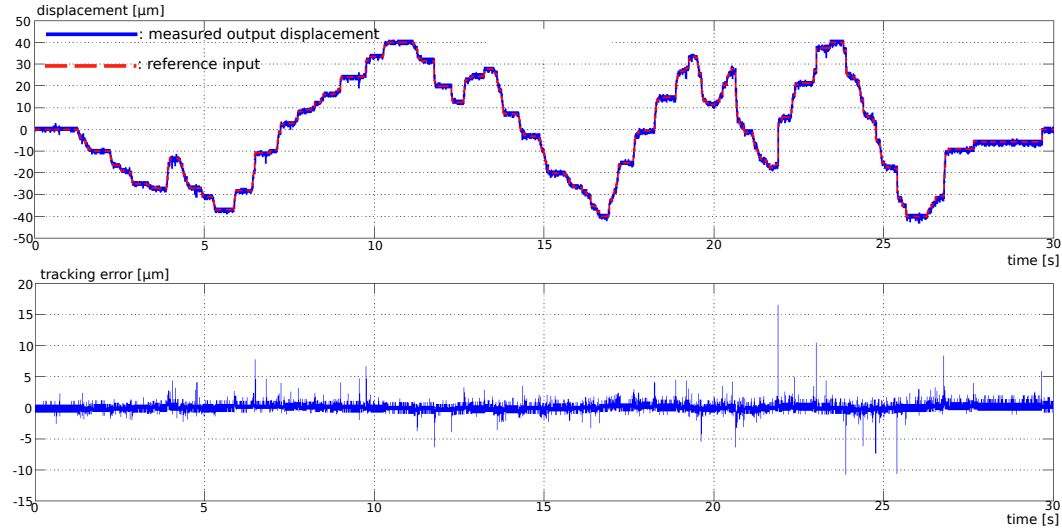


Fig. 14. (a): experimental response with varying input  $r_y$ . (b): tracking error.

The last experiment deals with the harmonic response of the suggested rate-dependent Prandtl-Ishlinskii (RDPI) feedforward controller combined with the internal model feedback controller (IMC). To demonstrate its interest, a IMC feedback-only scheme was also implemented. Furthermore, a feedforward combined with feedback scheme is also tested but, rather than using the RDPI compensator, we employ a rate-independent Prandtl-Ishlinskii (RIPI) compensator in the feedforward. To calculate the IMC feedback controller, the same specifications are used for the three schemes. These specifications are described above: settling time of  $t_r = 10ms$ , which corresponds to a desired

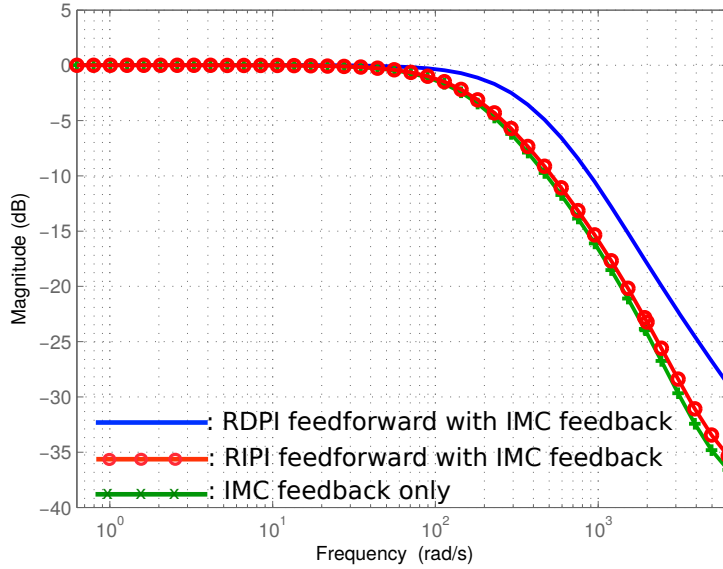
bandwidth of  $300\frac{rad}{s}$ . The experiments were carried out with a sine input reference  $r_y$  with an amplitude of  $40\mu m$  and a frequency ranging from less than  $0.1Hz$  where the creep is dominant to in excess of  $1kHz$  (in excess of  $6300\frac{rad}{s}$ ). Figure 14 displays the results. We observe that the suggested RDPI feedforward with IMC feedback scheme provides more bandwidth than the feedback only and than the RIPI feedforward combined with IMC feedback. In fact, the proposed rate-dependent hysteresis compensation permitted to handle both the nonlinearity and the dynamics of the actuator until certain frequency and thus helped the IMC feedback to have more bandwidth. In counterpart the rate-independent hysteresis compensation (RIPI) reduced the nonlinearity at one single frequency only (low frequency in this case:  $1Hz$ ). Hence, the RIPI combined with feedback behaves almost like the a feedback-only. We also checked the margins of the three schemes. All of them provided an infinite gain margin. However we observed that the suggested RDPI feedforward with IMC feedback scheme provided a larger phase margin relative to the two others schemes. Also, the RIPI feedforward with IMC feedback scheme provided a slight larger phase margin relative to the feedback-only scheme. Table 1 summarizes the bandwidths and the stability margins of the three schemes where it is evidenced that the suggested RDPI feedforward combined with the IMC feedback provides the best performances.

	bandwidth	gain margin	phase margin
RDPI feedforward + IMC feedback (suggested scheme)	$327\frac{rad}{s}$	$\infty dB$	$180deg$ (at $11.1\frac{rad}{s}$ )
RIPI feedforward + IMC feedback	$177\frac{rad}{s}$	$\infty dB$	$178deg$ (at $10.9\frac{rad}{s}$ )
feedback-only	$164\frac{rad}{s}$	$\infty dB$	$176deg$ (at $11\frac{rad}{s}$ )

Table 1  
*Performances evaluation.*

## 6 Conclusions

This paper dealt with the feedforward control of the rate-dependent hysteresis in smart materials based actuators. The RDPI (rate dependent Prandtl-Ishlinskii) model and compensator were therefore developed for that. A thorough analysis of the compensation error is afterwards developed. Then, we suggest to augment the feedforward scheme with a feedback control that is designed on the basis of this compensation error and of eventual model uncer-



(a)

Fig. 15. Frequency responses.

tainties. The internal model control scheme is suggested for this aim. Finally, the feedforward-feedback control scheme was applied to a piezoelectric actuator devoted to micromanipulation tasks. The experimental tests demonstrate the efficiency of the approach relative to feedback.

## Acknowledgment

This work was partially supported by the Labex-ACTION (ANR-11-LABX-0001-01). This work was also partially supported by the French “Investissements d’Avenir” program, project ISITE-BFC (contract ANR-15-IDEX-03).

## References

- [1] R. Smith, ‘Smart Material System: Model Development’, SIAM, 2005.
- [2] J. L. Pons, ‘Emerging Actuator Technology: A Micromechatronic Approach’, Wiley, 2005.
- [3] M. Rakotondrabe, ‘Smart Materials-Based Actuators at the Micro/Nano-Scale: Characterization, Control and Applications’, Springer-Verlag, New York, 2013.

- [4] S. Devasia, E. Eleftheriou, and S. O. R. Moheimani, 'A Survey of Control Issues in Nanopositioning', *IEEE Transactions on Control Systems Technology*, vol.15, no.5, pp.802-823, 2007.
- [5] A. Esbrook, X. Tan, and H. K. Khalil, 'Control of systems with hysteresis via servocompensation and its application to nanopositioning', *IEEE Transactions on Control Systems Technology*, vol.21, no.3, pp.725-738, 2013.
- [6] C. Visone, 'Hysteresis modelling and compensation for smart sensors and actuators', *Journal of Physics: Conference Series*, vol.138, no.1, 2008.
- [7] O. Aljanaideh, S. Rakheja, and C-Y. Su, 'Experimental characterization and modeling of rate-dependent asymmetric hysteresis of magnetostrictive actuators', *Smart Materials and Structures*, vol.23, no.3, doi:0964-1726-23-3-035002, 2014.
- [8] M. Al Janaideh and D. S. Bernstein, 'Inversion-free adaptive control of uncertain systems with SMA actuation', *proceedings of the American Control Conference*, pp.3585-3590, Washington, DC, 2013.
- [9] W. Oates, P. Evans, R. Smith, and M. Dapino, 'Experimental implementation of a hybrid nonlinear control design for magnetostrictive actuators', *Journal of Dynamic Systems, Measurement, and Control*, vol.131, no.4, 041004, 2009.
- [10] M. Al Janaideh, R. Naldi, L. Marconi, and P. Krejci, 'A hybrid system for a class of hysteresis nonlinearity: modeling and compensation', *Proceedings of the IEEE Decision and Control Conference*, Maui, HI, pp. 5380-5385, 2012.
- [11] William S. Oates, R. Zrostlik, S. Eichhorn, R. Smith, 'A Non-linear optimal control design using narrowband perturbation feedback for magnetostrictive actuators', *Journal of Intelligent Material Systems and Structures*, vol.21, pp.1681-1693, 2010.
- [12] A. El-Shaer, M. Al Janaideh, P. Krejci, and M. Tomizuka, 'Robust Performance Enhancement Using Disturbance Observers for Hysteresis Compensation based on Generalized Prandtl-Ishlinskii Model', *ASME Transactions of Journal of Dynamic Systems, Measurement, and Control*, vol.135, no.9, pp.1-13, 2013.
- [13] M. Al Janaideh, M. Rakotondrabe, and O. Aljanaideh, 'Further Results on Hysteresis Compensation of Smart Micropositioning Systems With the Inverse Prandtl-Ishlinskii Compensator', *IEEE Transactions on Control Systems Technology*, vol.24, no.2, pp.428-439, 2016.
- [14] M. Edarar, X. Tan, and H. K. Khalil, 'Sliding-mode tracking control of piezo-actuated nanopositioners', *Proceedings of the American Control Conference*, Montreal, QC, pp.3825-3830, doi: 10.1109/ACC.2012.6315559, 2012.
- [15] K. K. Leang and S. Devasia, 'Feedback-linearized inverse feedforward for creep, hysteresis, and vibration compensation in AFM piezoactuators', *IEEE Transactions on Control Systems Technology*, vol.15, no.5, pp.927-935, 2007.
- [16] X. Tan, J. S. Baras, 'Modeling and control of hysteresis in magnetostrictive actuators', *Automatica*, vol.40, no.9, pp.1469-1480, 2004.

- [17] S. K. Das, H. R. Pota and I. R. Petersen, 'Resonant controller design for a Piezoelectric tube scanner: A mixed negative-imaginary and small-gain approach', *IEEE Transactions on Control Systems Technology*, vol.22, no.5, pp.1899-1906, 2007.
- [18] G. Schitter, A. Stemmer, and F. Allgower, 'Robust 2 DOF-control of a piezoelectric tube scanner for high speed atomic force microscopy', *Proceedings of the American Control Conference*, vol.22, no.5, pp.3720-3725, 2003.
- [19] S. Yingfeng and K. Leang, 'Design and control for high-speed nanopositioning: serial-kinematic nanopositioners and repetitive control for nanofabrication', *IEEE Control Systems Magazine*, vol.33, no.6, pp.86-105, 2013.
- [20] M. Rakotondrabe, 'Classical Prandtl -Ishlinskii modeling and inverse multiplicative structure to compensate hysteresis in piezoactuators', *Proceedings of the American Control Conference*, Montreal, QC, pp. 1646-1651, 2012.
- [21] M. Rakotondrabe, 'Multivariable classical Prandtl-Ishlinskii hysteresis modeling and compensation and sensorless control of a nonlinear 2-dof piezoactuator', *Springer Nonlinear Dynamics*, DOI: 10.1007/s11071-017-3466-5, 2017.
- [22] M. Al Janaideh and P. Krejčí, 'Inverse rate-dependent Prandtl-Ishlinskii model for feedforward compensation of hysteresis in a piezomicropositioning actuator', *IEEE/ASME Transactions on Mechatronics*, vol.18, no.5, pp.1498-1507, 2013.
- [23] O. Aljanaideh, M. Al Janaideh, C-Y. Su, and S. Rakheja, 'Compensation of rate-dependent hysteresis nonlinearities in a magnetostrictive actuator using an inverse Prandtl-Ishlinskii model', *Smart Materials and Structures*, vol.22, no.2, doi:10.1088/0964-1726/22/2/025027, 2013.
- [24] M. Rakotondrabe, 'Bouc-Wen modeling and inverse multiplicative structure to compensate hysteresis nonlinearity in piezoelectric actuators', *IEEE Transactions on Automation Science and Engineering*, vol.8, no.2, pp.428-431, 2011.
- [25] D. Habineza, M. Rakotondrabe and Y. Le Gorrec, 'Multivariable generalized Bouc-Wen modeling, identification and feedforward control and its application to a 2-DoF piezoelectric multimorph actuator', *IFAC World Congress*, Cape Town, South Africa, pp.10952-10958, 2014.
- [26] D. Habineza, M. Rakotondrabe and Y. Le Gorrec, 'Bouc-Wen Modeling and Feedforward Control of multivariable Hysteresis in Piezoelectric Systems: Application to a 3-DoF Piezotube scanner', *IEEE Transactions on Control Systems Technology*, vol.23, no.5, pp.1797-1806, 2015.
- [27] R. Oubellil, L. Ryba, A. Voda, and M. Rakotondrabe, 'Experimental model inverse-based hysteresis compensation on a piezoelectric actuator', *International Conference on System Theory, Control and Computing*, Cheile Gradistei, Fundata Resort, Romania, pp.186-191, 2015.
- [28] Z. Li, C. Y. Su, T. Chai, 'Compensation of hysteresis nonlinearity in magnetostrictive actuators with inverse multiplicative structure for Preisach

model', IEEE Transactions on Automation Science and Engineering, vol.11, no.2, pp.613-619, April 2014.

- [29] O. Aljanaideh, M. Al Janaideh, and M. Rakotondrabe, 'Inversion-free feed-forward dynamic compensation of hysteresis nonlinearities in smart Micro/Nano- positioning actuators', IEEE Conference on Robotics and Automation, Seattle, WA, pp.2673-2678, 2015.
- [30] R.C. Smith and Z. Hu, 'The homogenized energy model for characterizing polarization and strains in hysteretic ferroelectric materials: Material properties and uniaxial model development', Journal of Intelligent Material Systems and Structures, vol.23, no.16, pp.1833-1867, 2012.
- [31] Z. Hu, R.C. Smith and J. Ernstberger, 'The homogenized energy model for characterizing polarization and strains in hysteretic ferroelectric materials: Implementation algorithms and data-driven parameter estimation techniques', Journal of Intelligent Material Systems and Structures, vol.23, no.16, pp.1869-1894, 2012.
- [32] M. Al Janaideh and P. Krejci, 'A Rheological model for the rate-dependent Prandtl-Ishlinskii model', Proceedings of the IEEE Conference on Decision and Control, Firenze, Italy, pp. 6646-6651, 2013.
- [33] M. Brokate and J. Sprekels, 'Hysteresis and Phase Transitions', New York, NY, Springer, 1996.
- [34] M. Rakotondrabe, K. Rabenoroso, J. Agnus and N. Chaillet, 'Robust feedforward-feedback control of a nonlinear and oscillating 2-dof piezocantilever', IEEE Transactions on Automation Science and Engineering, vol.8, no.3, pp.506-519, 2011.
- [35] M. Rakotondrabe, Y. Haddab, and P. Lutz, 'Quadrilateral modelling and robust control of a nonlinear piezoelectric cantilever', IEEE Transactions on Control Systems Technology, vol.17, no.3, pp.528-539, 2009.
- [36] M. Rakotondrabe, O. Aljanaideh and M. Al Janaideh, ' $H_\infty$  control for a smart micro-positioning system with an analytical model for the output of the inverse compensation', Proceedings of the American Control Conference, Chicago, IL, pp.2643-2648, 2015.
- [37] M. Edardar, X. Tan, and H. Khalil, 'Design and analysis of sliding mode controller under approximate hysteresis compensation', IEEE Transactions on Control Systems Technology, vol.23, no.2, pp.598-608, 2014.
- [38] J.A. Escareno, M. Rakotondrabe, and D. Habineza, 'Backstepping-based robust-adaptive control of a nonlinear 2-DOF piezoactuator', Control Engineering Practice, vol.41, pp.57-71, 2015.
- [39] L. Riccardi, D. Naso, B. Turchiano, and H. Janocha, 'Design of linear feedback controllers for dynamic systems with hysteresis', IEEE Transactions on Control Systems Technology, vol.22, no.4, pp.1268-1280, 2014.

- [40] J. Agnus, N. Chaillet, C. Clévy, S. Dembélé, M. Gauthier, Y. Haddab, G. Laurent, P. Lutz, N. Piat, K. Rabenorosoa, M. Rakotondrabe, and B. Tamadazte, 'Robotic Microassembly and micromanipulation at FEMTO-ST', *Journal of Micro-Bio Robotics*, vol.8, no.2, pp.91-106, 2013.
- [41] J. Rodriguez-Fortun, J. Orus, J. Alfonso, F. Gimeno, and J. Castellanos, 'Flatness -based active vibration control for piezoelectric actuators', *IEEE/ASME Transactions on Mechatronics*, vol.18, no.1, pp.221-229, 2013.
- [42] M. Rakotondrabe, 'Modeling and Compensation of Multivariable Creep in multi-DOF Piezoelectric Actuators', *IEEE Int Conference on Robotics and Automation*, pp.4577-4581, St Paul Minnesota USA, May 2012.
- [43] D. Habineza, M. Zouari, Y. Le Gorrec and M. Rakotondrabe, 'Characterization and modeling of the temperature effect on the piezoelectric tube actuator', *IFAC Symposium on Mechatronic*, pp.354-360, Loughborough University, UK, September 2016.
- [44] J. Schröck, T. Meurer and A. Kugi, 'Control of a flexible beam actuated by macro-fiber composite patches: II. Hysteresis and creep compensation, experimental results', *Smart Materials and Structures*, vol.20, no.1, 2010.
- [45] P-J. Koa, Y-P. Wanga, S-C. Tien, 'Inverse-feedforward and robust-feedback control for high-speed operation on piezo-stages', *International Journal of Control*, vol.86, num.2, 2013.
- [46] Y. Cao, S.K. Saskatoon, L. Cheng, X.B. Chen and J.Y. Peng, 'An Inversion-Based Model Predictive Control With an Integral-of-Error State Variable for Piezoelectric Actuators', *IEEE/ASME Trans. on Mechatronics*, vol.18, vol.3, 2013.
- [47] M. Rakotondrabe and Y. Le Gorrec, 'Force control in piezoelectric microactuators using self scheduled H-inf technique', *IFAC Symposium on Mechatronic*, pp.417:422, Cambridge Massachusetts USA, September 2010.
- [48] H.T. Banks, R.C. Smith and Y. Wang, 'Smart Material Structures: Modeling, Estimation and Control', Wiley-Blackwell, ISBN-13: 978-0471970248, 1996.
- [49] M. Rakotondrabe, A. Fowler, and S.O.R. Moheimani, 'Control of a novel 2-DoF MEMS nanopositioner with electrothermal actuation and sensing', *IEEE Transactions on Control Systems Technology*, vol.22, no.4, pp.1486-1497, 2014.